The Effects of Particle Size on the Adsorption of Metaldehyde by Oil Palm Kernel Biochar and Rice Husk Biochar

Nur Salsabila Kamarudin [1,2] , Farrah Aini Dahalan [1,2,*] , Masitah Hasan [1,2] , Naimah Ibrahim [1,2] , Nabilah Aminah Lutpi [1,2] , Raja Nazrul Hakim Raja Nazri [3] , Nor Azizah Parmin [4] , Achmad Syafiuddin [5]

[1] Centre of Excellence for Water Research and Environmental Sustainability Growth (WAREG), Universiti Malaysia Perlis (UniMAP), 02600 Arau, Perlis, Malaysia
[2] Faculty of Civil Engineering Technology, Universiti Malaysia Perlis (UniMAP), 02600 Arau, Perlis, Malaysia
[3] Universiti Kuala Lumpur, Branch Campus Malaysian Institute of Chemical and Bioengineering Technology, Melaka, Malaysia
[4] Institute of Nano Electronic Engineering (INEE), Universiti Malaysia Perlis, Lot 106, 108 & 110, Blok A, Taman Pertiwi Indah, Jalan Kangar-Alor Setar, Seriab 01000 Kangar, Perlis, Malaysia
[5] Department of Public Health, Universitas Nahdlatul Ulama Surabaya, 60237 Surabaya, East Java, Indonesia
* Correspondence: farrahaini@unimap.edu.my;

Abstract: Metaldehyde contamination poses risks to the environment and public health. Biochar, a carbon-rich material, is recognized for its potential to adsorb water pollutants. This study assesses the effectiveness of oil palm kernel biochar (OPKB) and rice husk biochar (RHB) in removing metaldehyde, considering particle sizes, initial concentrations, and contact times. Smaller biochar particles show increased adsorption sites with a porous structure, while larger particles have fewer active sites, impacting their efficiency. BET analysis reveals that the smallest biochar particles have higher specific surface areas ranging from 72.49 m^2/g to 123.08 m^2/g. OPKB1 proves to have the most effective adsorption capacity across all conditions. The experimental data are more consistent with the Freundlich isotherm model, which suggests that the active sites are not evenly distributed. The correlation coefficient (R^2) value indicates that the adsorption process is governed by pseudo-second-order kinetics.

Keywords: adsorption efficiency, isotherm, kinetics.

1. Introduction

Metaldehyde is a pesticide that is commonly used to control slugs and snails in agricultural and horticultural practices. Although its target is more specific than the commercially available molluscicides, it can still be toxic to non-target species, including mammals [1]. Both humans and animals have suffered from metaldehyde poisoning and death, according to some reports, although they are relatively rare compared to other types of pesticide poisoning [2, 3]. It is highly soluble in water and can easily contaminate surface and groundwater sources [4]. Metaldehyde is highly mobile in soils and can be detected in surface waters at concentrations above regulatory limits [5, 6]. This poses challenges for water

treatment plants, as conventional treatment processes are ineffective in removing metaldehyde [7]. Furthermore, metaldehyde can bioaccumulate over time, leading to long-term exposure and potential dysfunction in certain organs [8]. Metaldehyde can harm aquatic ecosystems and threaten human health if it contaminates water sources [9]. Therefore, developing effective methods for eliminating metaldehyde from water is essential.

Biochar is a material rich in carbon that can be obtained from biomass pyrolysis. It has attracted considerable interest as a potential adsorbent for eliminating various contaminants from water [9]. Biochar has a high surface area and a porous structure, providing ample contaminant adsorption site[10]. The ability of biochar to adsorb pollutants can be influenced by various factors, including the particle size of the biochar [11]. Biochar can serve as an adsorbent for eliminating pollutants from water and soil, including heavy metals, organic compounds, and pesticides [9]. Biochar derived from agricultural residuals was used to remove ammonium from water, and it was found that biochar had a strong attraction to various heavy metal ions, including pesticides, in water solutions [12]. Biochar derived from cotton gin waste and guayule bagasse was used to adsorb pharmaceuticals from water solutions, and the results show that biochar has high sorption coefficients for pesticides, including atrazine and simazine, indicating the potential of biochar for pesticide removal [13]. Biochar has a large surface area, a porous structure, and specific surface properties that enable it to adsorb pesticides and lower their concentration in water sources. These studies indicate that biochar can be a good adsorbent for pesticides, including metaldehyde. Hence, research on metaldehyde adsorption has a great chance of providing a substitute remedy for metaldehyde pollution.

Despite the potential of biochar as a low-cost and environmentally friendly adsorbent for metaldehyde removal, there is a lack of studies on how the particle size of biochar affects its adsorption performance and efficiency. The aim of this study is to examine how particle size affects the adsorption of metaldehyde by using oil palm kernel biochar and rice husk biochar. Specifically, the study aims to assess the adsorption capacities of oil palm kernel biochar and rice husk biochar for metaldehyde removal, comparing the adsorption performance of biochar particles with sizes < 0.3 mm, between 0.3 mm to 1 mm, and > 1 mm. The study also aims to determine the optimal adsorption of metaldehyde by manipulating the initial concentration of metaldehyde and contact time. It is important to know how the particle size influences the adsorption capacity of biochar to optimize its application as an adsorbent for metaldehyde elimination. This research contributes to optimizing biochar-based adsorption systems for effective metaldehyde remediation by elucidating the relationship between particle size and adsorption efficiency. The findings of this study will provide valuable insights into sustainable agricultural practices and the utilization of agricultural waste materials, such as oil palm kernel and rice husk biochar, for environmental remediation purposes.

2. Materials and Methods

2.1. Preparation of adsorbents.

Oil palm kernels were collected from local oil palm plantations, while rice husks were collected from local rice mills. The oil palm kernels and rice husks were cleaned thoroughly to get rid of dirt and debris. Any impurities, such as dust or stones, were removed through sieving. The cleaned oil palm kernels and rice husks undergo pyrolysis to convert them into biochar. The raw oil palm kernels and raw rice husks were loaded into a pyrolysis reactor and heated in an oxygen-limited environment at 600°C for 4 hours, with a heating rate of less than 10°C. The

biochar was allowed to naturally cool down at room temperature to ensure the preservation of its properties. The obtained oil palm kernel biochar and rice husk biochar were sieved to get particle sizes smaller than 0.3 mm, between 0.3 to 1 mm, and larger than 1mm. This was achieved by passing the biochar through appropriately sized mesh sieves. The sieved biochar particles were collected, and any oversized or undersized particles were removed. Figure 2.1 shows the sieved oil palm kernel biochar (OPKB) and rice husk biochar (RHB) with sizes ranging from less than 0.3 mm, 0.3 to 1 mm, and more than 1 mm. The sieved biochar was washed with distilled water and dried in an oven at 80°C overnight. Then, the dried biochar was labeled and stored accordingly in an airtight container to maintain its quality until further use. Table 2.1 shows the type of sample, particle size, and label name for each sample.
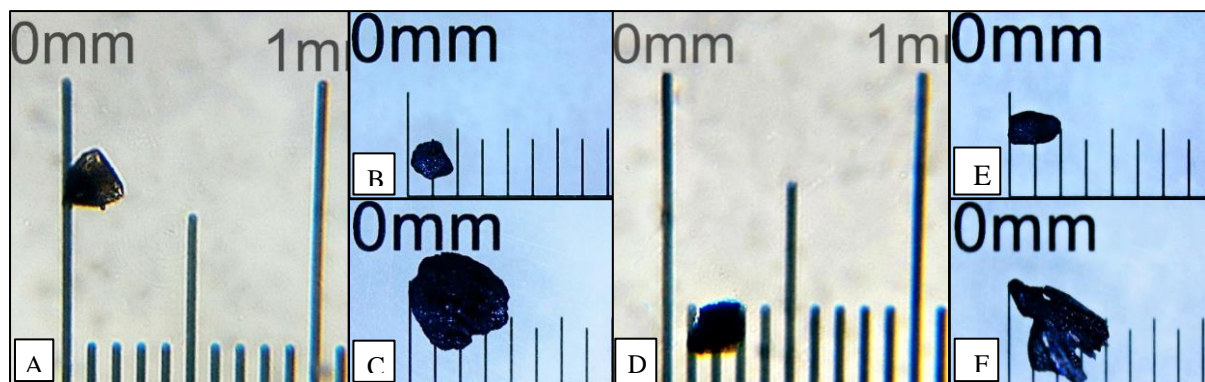

Figure 1. The size of (**A**) OPKB1 under 40x compound microscope, (**B**) OPKB2; (**C**) OPKB3; (**D**) RHB1 under 40x compound microscope; (**E**) RHB2; (**F**) RHB3.

Table 1. Summary of the parameters in batch adsorption.

Type of sample	Particle size	Label name
Oil palm kernel biochar	<0.3mm	OPKB1
	0.3mm-1mm	OPKB2
	>1mm	OPKB3
Rice husk biochar	<0.3mm	RHB1
	0.3mm-1mm	RHB2
	>1mm	RHB3

2.2. Preparation of metaldehyde.

The reference method from the UK Environment Agency was used to prepare the metaldehyde stock solution. A total of 0.1 g Metaldehyde powder (Sigma-Aldrich, USA) was added to 100 mL methanol to make a 10 ppm metaldehyde stock solution. The stock solution was thoroughly mixed to ensure the complete dissolution of metaldehyde. The metaldehyde stock solutions could be kept between 1°C and 10°C for up to 1 year. Deionized water was utilized as a solvent to prepare different concentrations of metaldehyde. A series of dilutions were prepared from the metaldehyde stock solution to establish a standard curve for metaldehyde quantification. The dilutions covered a range of concentrations, including above and below the expected concentration range of the samples. The dilutions were prepared by carefully pipetting an appropriate volume of the stock solution into a series of volumetric flasks containing a known volume of deionized water. Each dilution was mixed thoroughly to obtain a homogeneous solution.

2.3. Characterization of adsorbents.

The OPKB and RHB prepared for this study undergo a characterization process to determine their structural and surface properties. The biochar samples were attached to

Scanning Electron Microscopy (SEM) stubs and coated with platinum to improve their surface conductivity. Scanning electron microscopy was conducted using the JSM-6010LA InTouchScope™ Multiple Touch Panel SEM. The biochar samples were examined at various magnifications to visualize the fine and coarse biochar particles' morphology, particle shape, and surface features. SEM images were captured, and representative images were selected for analysis and inclusion in the study. The SEM images were qualitatively analyzed to assess the differences in particle size, surface morphology, and structural characteristics between the fine and coarse biochar particles.

The Brunauer-Emmett-Teller (BET) analysis technique was used to measure the biochar samples' specific surface area and porosity. Before analysis, the biochar samples were degassed under vacuum at elevated temperatures to remove adsorbed gases or moisture. BET analysis was performed using a gas adsorption instrument. At different relative pressures, nitrogen gas adsorption isotherms were measured. The BET analysis data were put through the right mathematical models, like the BET equation, to determine the biochar samples' specific surface area, pore size distribution, and total pore volume.

2.4. Batch adsorption studies.

To examine the effect of the initial concentration of metaldehyde, 100mL of metaldehyde solutions of varying concentrations were poured into separate 250 mL conical flasks. Each flask received 1g of adsorbents. The biochar and metaldehyde solutions were completely mixed on an orbital shaker at 150 rpm for 150 minutes to ensure appropriate contact. In separate 250 mL conical flasks, a 100 mL solution of metaldehyde with an initial concentration of 0.01 ppm and 1g of adsorbents was prepared in batches to examine how contact time influences the outcome. The biochar samples were mixed with metaldehyde solutions and shaken for the desired contact times (1 to 180 minutes). A set of conical flasks with adsorbates without biochar was utilized as a control. To prevent evaporation, all the flasks were covered with parafilm. After each adsorption process, filtration separated the adsorbents from the metaldehyde solution. This batch adsorption technique was carried out in triplicate to ensure precision and consistency. Table 2 depicts the parameters of the procedure. The concentration of metaldehyde in the filtered solution was quantified with a UV-visible spectrophotometer at 270nm spectra. The utilization of quartz cuvettes in metaldehyde analysis via UV-visible spectrophotometry enhances the quality and reliability of the analytical process.

Table 2. Summary of the parameters in batch adsorption.

Parameters	Range
Initial concentration	0.001, 0.01, 0.1, 0.5, 1, 2, 3, 4, 5, 7ppm
Contact time	1, 5, 10, 20, 30, 60, 90, 120, 150, and 180 minutes

2.5. Isotherm and kinetic studies.

The Langmuir and Freundlich isotherms and the first-order and second-order kinetics clarify the adsorption behavior. Table 3 depicts the formula for both isotherm and kinetic models utilized in this study. The Langmuir isotherm, which presupposes a monolayer adsorption mechanism on a homogenous surface, provides insights into the maximum adsorption capacity (Q_m) and the energy of adsorption (b). In contrast, the Freundlich isotherm allows for a more realistic representation of heterogeneous surfaces with a multilayer adsorption mechanism characterized by the adsorption capacity (K_F) and the Freundlich exponent (n). The adsorption process is investigated through first-order and second-order

models, which give information about the rate constants (k_1 and k_2) and shed light on the underlying mechanisms of metaldehyde adsorption over time.

Table 3. Mathematical models used in the adsorption study.

	Model	Equation
Isotherm	Langmuir	$q_e = \dfrac{q_m.b.C_e}{1 + b.C_e}$
	Freundlich	$\log q_e = \log k_f + \dfrac{1}{n}.\log C_e$
Kinetic	Pseudo-first-order	$\log(q_e - q_t) = \log q_e - \dfrac{k_1}{2.303}.t$
	Pseudo-second-order	$q_t = \dfrac{q_e^2.k_2.t}{1 + q_e.k_2.t}$

3. Results and Discussion

3.1. Characterization of biochar.

Figure 2 reveals distinct variations in the surface morphology of biochar particles of varying sizes. OPKB and RHB, with less than 0.3 mm and 0.3 mm to 1 mm, were observed to exhibit a more pronounced porous structure and a greater number of finer pores across the biochar surface. This particle size has a very porous and rough surface. The pores are small and irregular in shape. [14] also, a fine-size-fractionated sunflower husk biochar was revealed to have a porous morphology with a pronounced porous structure and finer pores across the biochar surface. This outcome matches the principle that smaller particles' surface area per unit mass is greater, leading to a higher density of pores and potential adsorption sites. The finer pores observed in smaller particles also imply enhanced affinity for adsorbates, crucial for efficient adsorption processes. Conversely, OPKB and RHB sizes greater than 1mm displayed a relatively less intricate porous network with larger and more irregularly shaped pores. The coarser surface morphology of larger particles might be attributed to a reduced surface area-to-volume ratio. These observations align with the concept that larger particles have limited surface exposure and fewer active adsorption sites, potentially contributing to decreased adsorption efficiency.

Table 3 shows the BET results for all particle sizes of OPKB and RHB. Based on the results, OPKB and RHB with particle sizes less than 0.3mm have the highest bet surface area, with 123.08 m^2/g and 72.49 m^2/g, respectively. The results show that the specific surface area of the smaller particle sizes is higher than that of the larger particle sizes. This was supported by [15], who highlighted that smaller biochar particles have a greater specific surface area per unit of mass. The smaller particle sizes possess a larger exposed surface area, which explains this. The outcome of the BET analysis indicated a clear relationship between particle size and specific surface area. Smaller particle sizes of biochar consistently exhibited a significantly larger specific surface area compared to their larger counterparts. This finding is in line with the general principle that reducing particle size leads to an increase in the available surface area per unit mass. The greater surface area of smaller particles implies the presence of more active sites for adsorption interactions, potentially resulting in improved adsorption capacities for various adsorbates.

The BET isotherms obtained from the analysis further provided insights into biochar particles' porosity and pore structure. Smaller particle sizes displayed steeper adsorption isotherms, indicative of a higher degree of porosity and greater available pores. The increased porosity of smaller particles means that adsorbates can reach the internal pore structure more

easily. This makes mass transfer and adsorption processes go faster and work better. The larger specific surface area and enhanced porosity of smaller particles suggest that they are more suitable for adsorption processes requiring rapid and efficient adsorbate uptake. Additionally, more sites for adsorption could result in higher adsorption capacities, making smaller biochar particles desirable for environmental remediation, water treatment, and other adsorption-based applications. Conversely, larger particle sizes were associated with reduced specific surface area and porosity. This might indicate a limitation in the number of available adsorption sites and slower mass transfer, which could impact the overall adsorption performance.
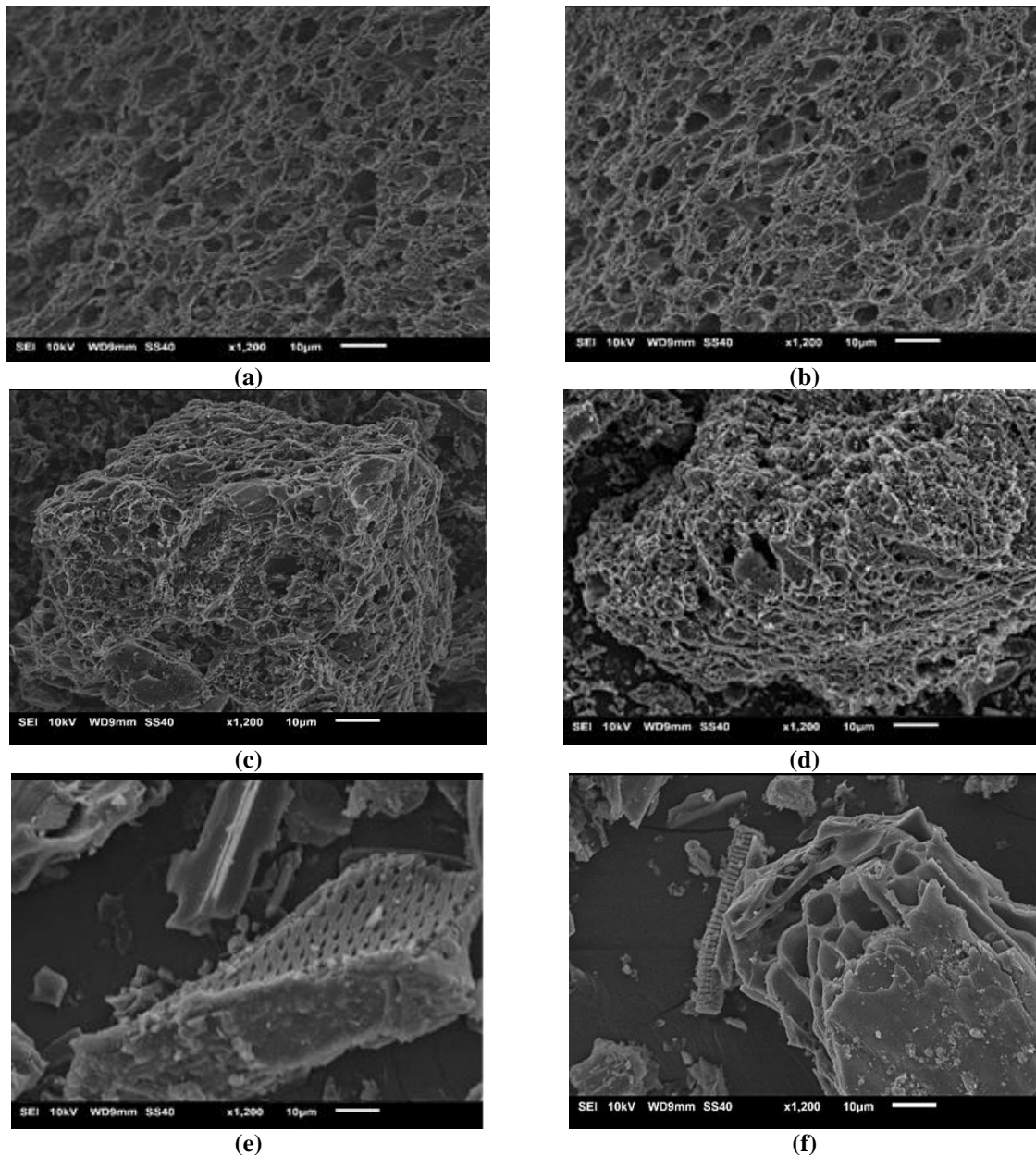
Figure 2. The SEM image of **(a)** OPKB1; **(b)** OPKB2; **(c)** OPKB3; **(d)** RHB1; **(e)** RHB2; **(f)** RHB3.

Table 3. The summary of BET surface area, Total pore volume, and porosity for all adsorbents.

Type of biochar	Particle size	Bet surface area (m²/g)	Total pore volume (cm³/g)	Porosity
Oil palm kernel biochar	< 0.3mm	123.08	0.43	0.96
	0.3mm-1mm	34.19	0.12	0.95
	> 1mm	27.16	0.08	0.95
Rice husk biochar	< 0.3mm	72.49	0.23	0.95
	0.3mm-1mm	17.10	0.05	0.94
	> 1mm	7.84	0.03	0.94

The BET results tally with previous studies as [16] discuss how the BET surface area of biochar changes with smaller particle sizes. The main point of this study was that the surface area of biochar grew to smaller sizes. The effect of biochar particle size on available water capacity (AWC) is also revealed by [17]. It was reported that AWC is higher for smaller biochar particle sizes (<0.5 mm) than for larger particle sizes (>1 mm).

3.2. Batch adsorption of metaldehyde.

Based on Figure 3 (A), it was observed that the percentage of metaldehyde adsorbed by biochar increased with increasing concentration. OPKB1 exhibits the highest percentage of adsorption efficiency in all initial concentrations tested, followed by OPKB2 and OPKB3. On the other hand, RHB1, RHB2, and RHB3 exhibit a slightly lower percentage of metaldehyde removed from the sample. This means that OPKB1 is the most effective adsorbent at all ranges of initial concentrations of metaldehyde. In the case of a lower concentration of metaldehyde, the reaction rate is lowered and can be increased by increasing the initial concentration of metaldehyde up to 2 ppm. Beyond this concentration, however, the available surface area is lowered, and the percentage of metaldehyde removal is hardly increasing. The concentration affects the available driving force for the transfer of metaldehyde ions onto the adsorbent particles. The driving force is low at low concentrations but rises at high concentrations. This improves the interaction between the metaldehyde ions in the aqueous phase and the active sites of the adsorbents. This causes an increase in the uptake of metaldehyde ions.
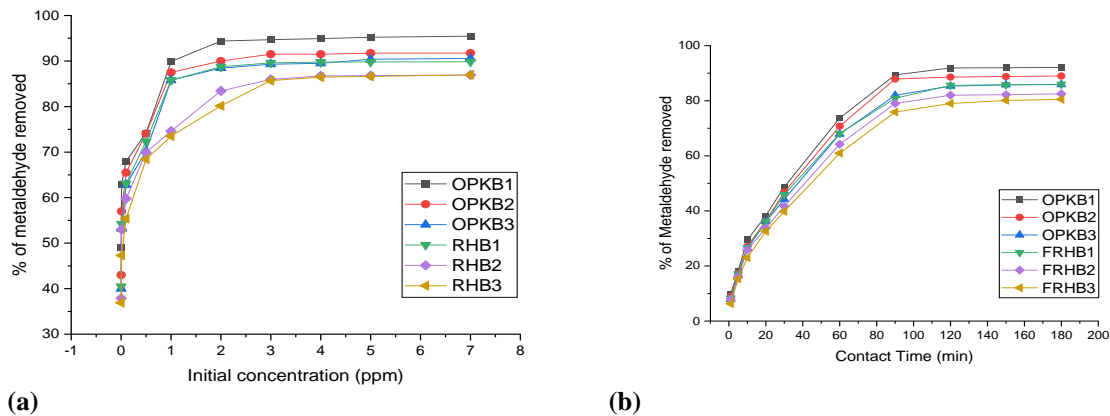

(a)   **(b)**

Figure 3. The graph of **(a)** the effect of initial concentration on the percentage of metaldehyde removed; **(b)** the effect of contact time on the percentage of metaldehyde removed.

The increased surface area of smaller particles, which offers more active adsorption sites, explains particle size's effect on adsorption [18, 19]. The surface area of smaller particle sizes is greater, enabling a higher adsorption capacity. This matches the results of previous studies that have demonstrated a higher adsorption capacity for adsorbents with smaller particle sizes [18]. Additionally, smaller particle sizes have been found to enhance the adsorption efficiency of dyes in wastewater treatment.

Based on Figure 3.2(B), once again, OPKB1 exhibits the highest percentage of metaldehyde removed, followed by OPKB2 and OPKB3 at all contact times. All rice husk biochar has a slightly lower percentage of adsorption capacity for metaldehyde than oil palm kernel biochar. It is evident that all adsorbents showed rapid metal adsorption within 90 minutes of contact time due to the easy accessibility of the adsorption sites on the adsorbent, which was followed by a constant adsorption rate at longer contact times.

One of the possible causes of this result is equilibrium attainment. Increasing the contact time allows more time for the adsorbate to come into contact with the adsorbent and

reach equilibrium [20-28]. As the contact time increases, more metaldehyde molecules can interact with the active sites on the surface of the biochar, leading to increased adsorption. In addition, active site availability can also influence the adsorption rate. With longer contact times, the adsorbate molecules have a higher chance of encountering and binding to the available active sites on the biochar surface [18]. This results in a higher percentage of metaldehyde being adsorbed onto the biochar. Increasing the contact time allows for more efficient diffusion and penetration of metaldehyde into the porous structure of the biochar [21]. As the contact time increases, metaldehyde molecules have more time to diffuse into the internal pores of the biochar, leading to increased adsorption capacity. There may be a point of saturation where further increases in contact time do not significantly increase adsorption [26]. This occurs when the active sites on the biochar surface become fully occupied by metaldehyde molecules, and no additional adsorption can take place.

Based on both results, it can be assured that oil palm kernel biochar exhibits the highest adsorption capacity compared to rice husk biochar. Biochar produced from oil palm kernel shells has been found to have favorable physicochemical properties for pollutant adsorption. For example, oil palm kernel biochar has been shown to have a higher concentration of base cations, which can enhance the removal of pollutants like cadmium from aqueous solutions [27]. On the other hand, rice husk biochar may have lower concentrations of these base cations, leading to lower adsorption capacities. It has been observed that the surface acid functional groups on biochar, which are important for adsorption, can vary depending on the feedstock and pyrolysis conditions [28]. The presence of these functional groups can enhance the adsorption of pollutants. Studies have shown that oil palm kernel biochar produced at certain temperatures can have higher surface acid functional group concentrations than rice husk biochar, leading to improved adsorption efficiency.

Furthermore, biochar's surface area and pore structure are crucial factors in adsorption processes [28]. Oil palm kernel biochar has been found to have a greater surface area and pore volume compared to rice husk biochar, providing more active sites for pollutant adsorption [29]. The larger surface area of oil palm kernel biochar allows for more interactions between the biochar and pollutants, leading to higher adsorption capacities. Moreover, the presence of certain elements and compounds in the feedstock can also contribute to the adsorption efficiency of biochar. For example, oil palm kernel shells contain high levels of inorganic nutrients, which can enhance the adsorption capabilities of the resulting biochar [30]. These nutrients can act as additional binding sites for pollutants, increasing the adsorption capacity.

3.3. Isotherm and kinetics of metaldehyde adsorption.

The adsorption isotherm refers to the distribution of adsorbate molecules between the liquid and solid phases when the adsorption process reaches equilibrium [31]. It describes the relationship between the amount of adsorbate adsorbed onto the adsorbent and the equilibrium concentration of the adsorbate in the solution [32]. Adsorption isotherms are commonly used to analyze and predict a particular system's adsorption behavior and determine the adsorbent's maximum adsorption capacity. Figure 3.3 shows the graph of Langmuir and Freundlich isotherms for all samples.
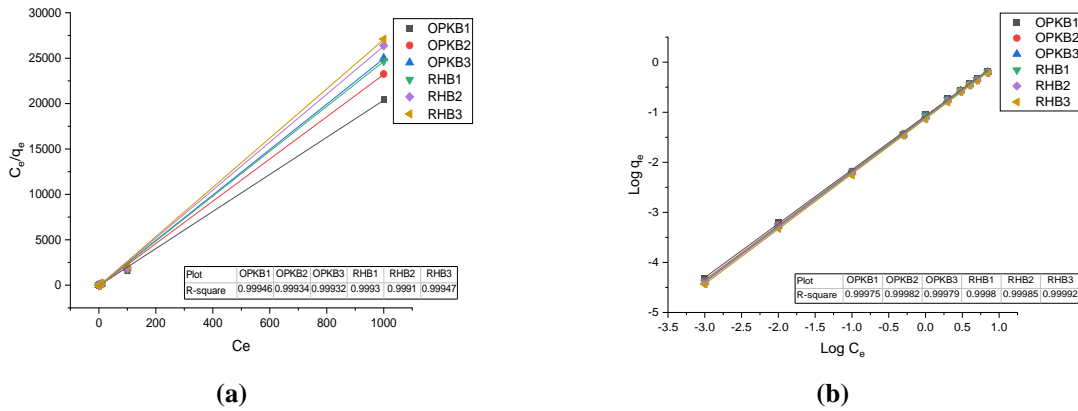
Plot	OPKB1	OPKB2	OPKB3	RHB1	RHB2	RHB3
R-square	0.99946	0.99934	0.99932	0.9993	0.9991	0.99947

Plot	OPKB1	OPKB2	OPKB3	RHB1	RHB2	RHB3
R-square	0.99975	0.99982	0.99979	0.9998	0.99985	0.99992

| (a) | (b) |

Figure 4. The plot of **(a)** C_e versus C_e/q_e of Langmuir isotherm; **(b)** Log C_e versus Log q_e of Freundlich isotherm.

Figure 4(A) shows the plot of C_e versus C_e/q_e, which represents the Langmuir isotherm behavior for the adsorption of metaldehyde by OPKB1, OPKB2, OPKB3, RHB1, RHB2, and RHB3. It can be deduced from the graph using the correlation coefficient (R^2) values that the experimental data for all samples does not fit into the Langmuir isotherm model. Although all samples resulted in a correlation coefficient greater than 0.999, it is proven that Freundlich isotherms generate a higher correlation coefficient than Langmuir isotherms. The non-applicability of the Langmuir isotherm indicates negative monolayer coverage of metaldehyde ions on the surface of adsorbents, which suggests the non-formation of a monolayer on the adsorbent surface in the given concentration range. The fact that the Langmuir isotherm does not fit the experimental data may be due to the non-homogenous distribution of active sites on the adsorbent since the Langmuir equation assumes that the surface is homogenous.

Figure 4(B) shows the Log Ce versus Log qe graph, which represents the Freundlich isotherms in an adsorption system, comparing the correlation coefficient values for the adsorption of metaldehyde on the adsorbents. Based on the plot, all samples fit the Freundlich isotherm with a correlation coefficient greater than 0.99975. Based on the result, RHB3 shows the highest R^2 value with 0.99992, followed by RHB2 with 0.99985. If the correlation coefficient is higher in the Freundlich isotherm, it indicates a better-fitting model compared to the Langmuir isotherm. A higher correlation coefficient suggests that the experimental data agrees well with the Freundlich adsorption isotherm model [35-40]. This implies that the Freundlich isotherm provides a more accurate representation of the adsorption process and the behavior of the adsorbate on the adsorbent surface.

The Freundlich isotherm is commonly used to describe heterogeneous adsorption systems where adsorption occurs on multiple sites with different affinities and energies. It assumes a non-ideal adsorption process and reversible molecule interactions [34]. The Freundlich equation is exponential and can be applied in the low to intermediate concentration ranges [39]. The higher correlation coefficient in the Freundlich isotherm suggests that the adsorption process is more predominant and can be described by multilayer adsorption on the heterogeneous surface of the adsorbent [40].

Adsorption kinetics, on the other hand, refers to the rate at which the adsorption process occurs [41, 42]. It involves studying the time-dependent adsorption behavior and determining the rate at which the adsorbate molecules bind to the adsorbent surface [43]. Kinetic models, such as pseudo-first-order (PFO) and pseudo-second-order (PSO) models, are used to describe and analyze the adsorption kinetics [41]. These models help to understand the mechanism and rate of adsorption as well as predict the adsorption capacity at different time intervals. A study

of the kinetics of solute uptake is desirable as it provides information about the mechanisms of adsorption, which is important for the efficiency of the process. In addition, information on adsorption kinetics is required to select the optimum operating conditions for a full-scale batch process.

Using PFO and PSO kinetic models, the rate at which metaldehyde binds to OPKB and RHB was studied. The adsorption kinetics described the rate of metaldehyde adsorption on these adsorbents as a function of time. It helps to determine equilibrium time, which gives useful information about the design of the adsorption process and pollution flux. The closeness of the experimental data and the model-predicted values was expressed by the correlation coefficient (R^2). A relatively high R^2 value implies that the model successfully illustrates the kinetics of metaldehyde adsorption. Figure 5 shows the plot of PFO and PSO. Based on the results, it can be assured that this adsorption system fits well with the PSO, as all adsorbents have a correlation coefficient greater than 0.98. The results obtained suggest that the adsorption of metaldehyde onto biochar fits the PSO, which assumes that the rate-limiting step may be chemisorption.
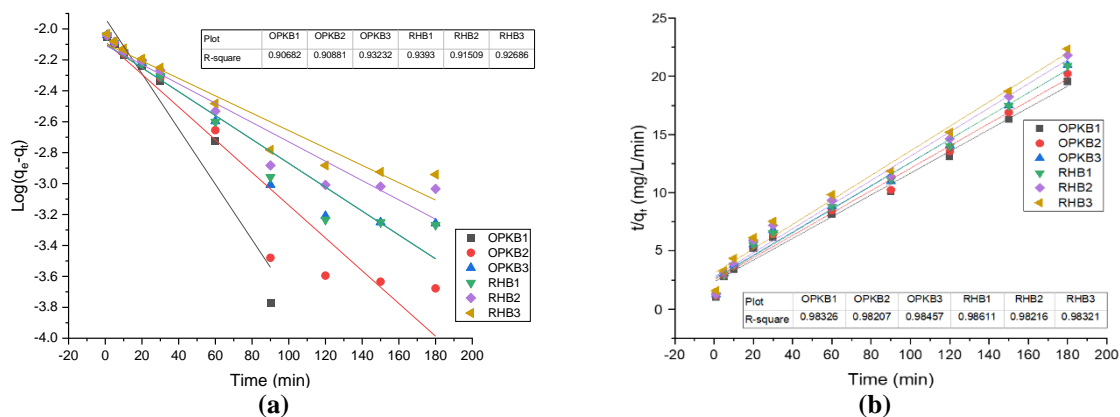

Figure 5. The plot of **(a)** time versus Log (q_e-q_t) of pseudo-first-order; **(b)** time versus t/q_t of pseudo-second-order.

The chemical interactions between the adsorbate and adsorbent suggest that the rate-limiting step of the adsorption process is the formation of chemical bonds or surface complexation [44, 45]. The PSO model assumes that the adsorption rate is proportional to the square of the concentration of the adsorbate and the number of available adsorption sites on the adsorbent surface [44]. This is consistent with the chemisorption mechanism, where the adsorbate molecules undergo strong chemical bonding with the adsorbent surface. The PSO model is often observed when the adsorption process is irreversible, and the adsorbent has a stable structure [45]. This indicates that the adsorption process is irreversible, and the adsorbate molecules are strongly bound to the adsorbent surface. The PSO model is often observed when the adsorption process reaches equilibrium relatively quickly [44]. This suggests that the adsorption process is rapid, and equilibrium is achieved within a short period of time. Furthermore, the PSO model is often observed when the adsorbent's adsorption capacity and the adsorbate's intrusion into its structure depend on the reaction time of the adsorptive [45]. This indicates that the reaction conditions and the properties of the adsorbent and adsorbate influence the adsorption process.

This result is also supported by previous studies by [46] in which the adsorption of phosphorus in soil incubated with biochar was studied, and the PSO model fitted well to the adsorption kinetics, indicating that the adsorption process is chemically controlled. Furthermore, [47] investigated the adsorption of Acid Red 88 dye using biochar and found that

the adsorption process followed the PSO kinetic model, suggesting a chemisorption mechanism. In addition, [48] compared the PFO and PSO kinetic models for the adsorption of Cd ions by biochar and found that the PSO model provided a better fit to the experimental data, indicating that the chemisorption mechanism mainly controls the adsorption rate of biochar.

4. Conclusions

In conclusion, this thorough study looked at how particle size and adsorption efficiency interact in the case of metaldehyde adsorption using OPKB and RHB. The discernible prominence of smaller particle-size biochar in demonstrating heightened adsorption efficacy underscores its pivotal role in optimizing pollutant removal strategies. Moreover, the consistently superior adsorption efficiency of OPKB as compared to RHB highlights the critical influence of biochar type on adsorption performance. The corroborative fit of the Freundlich isotherm model to the adsorption system illuminates the adsorption process's heterogeneous nature, and the adsorption kinetics' alignment with the PSO model reaffirms the underlying mechanism of chemisorption. This study contributes to the ever-evolving understanding of the complex factors that govern adsorption processes, thereby presenting a promising avenue for tailoring efficient and sustainable water treatment methods. Prospective research endeavors could further probe the nuances of biochar characteristics, elucidate their synergistic effects on adsorption performance, and explore real-world applications to address emerging environmental challenges.

Funding

Acknowledgments

Conflicts of Interest

The authors declare no conflict of interest.

References

1. Plan, M.R.R.; Saska, I.; Cagauan, A.G.; Craik, D.J. Backbone Cyclised Peptides from Plants Show Molluscicidal Activity against the Rice Pest Pomacea canaliculata (Golden Apple Snail). *J. Agric. Food Chem.* **2016**, *56*, 5237–5241, https://doi.org/10.1021/jf800302f.
2. Maher, S.; Jjunju, F.P.M.; Damon, D.E.; Gorton, H.; Maher, Y.S.; Syed, S.U.; Heeren, R.M.A.; Young, I.S.; Taylor, S.; Badu-Tawiah, A.K. Direct Analysis and Quantification of Metaldehyde in Water using Reactive Paper Spray Mass Spectrometry. *Sci. Rep.* **2016**, *6*, 35643, https://doi.org/10.1038/srep35643.
3. Botelho, A.F.M.; Machado, A.M.D.; da Silva, R.H.S.; Faria, A.C.; Machado, L.S.; Santos, H.; Braga, S.d.M.; Torres, B.B.J.; Miguel, M.P.; Chaves, A.R.; Melo, M.M. Fatal metaldehyde poisoning in a dog confirmed by gas chromatography. *BMC Vet. Res.* **2020**, *16*, 139, https://doi.org/10.1186/s12917-020-02348-w.
4. Rolph, C.A.; Jefferson, B.; Hassard, F.; Villa, R. Metaldehyde removal from drinking water by adsorption onto filtration media: mechanisms and optimization. *Environ. Sci.: Water Res. Technol.* **2018**, *4*, 1543–1552, https://doi.org/10.1039/c8ew00056e.

5. Ramos, M.; Gomes, S.R.; Gutierrez, Y.; Ramos-Rodriguez, O.; Uzeda, M.C. Terrestrial Slugs in Neotropical Agroecosystems. *Front. Sustain. Food Syst.* **2021**, *5*, 656492, https://doi.org/10.3389/fsufs.2021.656492.

6. Castle, G.D.; Mills, G.A.; Gravell, A.; Leggatt, A.; Stubbs, J.; Davis, R.; Fones, G.R. Comparison of different monitoring methods for the measurement of metaldehyde in surface waters. *Environ. Monit. Assess.* **2019**, *191*, 75, https://doi.org/10.1007/s10661-019-7221-x.

7. Castle, G.D.; Mills, G.A.; Bakir, A.; Gravell, A.; Schumacher, M.; Townsend, I.; Jones, L.; Greenwood, R.; Knott, S.; Fones, G.R. Calibration and field evaluation of the Chemcatcher® passive sampler for monitoring metaldehyde in surface water. *Talanta* **2018**, *179*, 57–63, https://doi.org/10.1016/j.talanta.2017.10.053.

8. Saad, A.M.; Ismail, S.W.; Dahalan, F.A. METALDEHYDE TOXICITY: A BRIEF ON THREE DIFFERENT PERSPECTIVES. *J. Civ. Eng. Sci. Technol.* **2017**, *8*, 108–114, https://doi.org/10.33736/jcest.444.2017.

9. Li, Z.; Kim, J.K.; Chaudhari, V.; Mayadevi, S.; Campos, L.C. Degradation of metaldehyde in water by nanoparticle catalysts and powdered activated carbon. *Environ. Sci. Pollut. Res.* **2017**, *24*, 17861-17873, https://doi.org/10.1007/s11356-017-9249-1.

10. Saarela, T.; Lafdani, E.K.; Laurén, A.; Pumpanen, J.; Palviainen, M. Biochar as adsorbent in purification of clear-cut forest runoff water: adsorption rate and adsorption capacity. *Biochar* **2020**, *2*, 227–237, https://doi.org/10.1007/s42773-020-00049-z.

11. Shen, Z.; Jin, F.; Wang, F.; McMillan, O.; Al-Tabbaa, A. Sorption of lead by Salisbury biochar produced from British broadleaf hardwood. *Bioresour. Technol.* **2015**, *193*, 553-556, https://doi.org/10.1016/j.biortech.2015.06.111.

12. Gao, F.; Xue, Y.; Deng, P.; Cheng, X.; Yang, K. Removal of aqueous ammonium by biochars derived from agricultural residuals at different pyrolysis temperatures. *Chem. Speciat. Bioavailab.* **2015**, *27*, 92-97, https://doi.org/10.1080/09542299.2015.1087162.

13. Ndoun, M.C.; Elliott, H.A.; Preisendanz, H.E.; Williams, C.F.; Knopf, A.; Watson, J.E. Adsorption of pharmaceuticals from aqueous solutions using biochar derived from cotton gin waste and guayule bagasse. *Biochar* **2021**, *3*, 89-104, https://doi.org/10.1007/s42773-020-00070-2.

14. Gluba, Ł.; Rafalska-Przysucha, A.; Szewczak, K.; Łukowski, M.; Szlązak, R.; Vitková, J.; Kobyłecki, R.; Bis, Z.; Wichliński, M.; Zarzycki, R.; Kacprzak, A.; Usowicz, B. Effect of Fine Size-Fractionated Sunflower Husk Biochar on Water Retention Properties of Arable Sandy Soil. *Materials* **2021**, *14*, 1335, https://doi.org/10.3390/ma14061335.

15. Blanco-Canqui, H. Biochar and Soil Physical Properties. *Soil Sci. Soc. Am. J.* **2017**, *81*, 687–711, https://doi.org/10.2136/sssaj2017.01.0017.

16. Lonappan, L.; Rouissi, T.; Kaur Brar, S.; Verma, M.; Surampalli, R.Y. An insight into the adsorption of diclofenac on different biochars: Mechanisms, surface chemistry, and thermodynamics. *Bioresour. Technol.* **2018**, *249*, 386-394, https://doi.org/10.1016/j.biortech.2017.10.039.

17. Edeh, I.G.; Mašek, O.; Buss, W. A meta-analysis on biochar's effects on soil water properties – New insights and future research challenges. *Sci. Total Environ.* **2020**, *714*, 136857, https://doi.org/10.1016/j.scitotenv.2020.136857.

18. Zikri, R.; Natasyah, E.; Muhdarina, M. Synthesis of Oil Palm Fronds Charcoal as Adsorbent to Reduce Levels of Fe (III) in Peat Water. *J. Kim. Sains Apl.* **2022**, *25*, 300–306, https://doi.org/10.14710/jksa.25.8.300-306.

19. Abazli, H.; Jneidi, H.; Hatem, S. Kinetic, Isotherm and Thermodynamic Studies on the Ciprofloxacin Adsorption from Aqueous Solution Using Aleppo bentonite. *Baghdad Sci. J.* **2022**, *19*, 0680-0680, https://doi.org/10.21123/bsj.2022.19.3.0680.

20. Akpan, O.-O.P.; Etuk, B.R. Adsorption of Cyanide from Cassava Wastewater Using Calcined and Activated Oyster Shell Ash. *J. Eng. Res. Rep.* **2019**, *6*, 1–9, https://doi.org/10.9734/jerr/2019/v6i116938.

21. Batool, F.; Irfan, A.; Al-Hussain, S.A.; Al-Farraj, E.S.; Iqbal, S.; Akbar, J.; Noreen, S.; Akhtar, T.; Iqbal, T.; Zaki, M.E.A. Development of Ion Character Property Relationship (IC-PR) for Removal of 13-Metal Ions by Employing a Novel Green Adsorbent *Aerva javanica*. *Molecules* **2022**, *27*, 8213, https://doi.org/10.3390/molecules27238213.

22. Tandorn, S.; Arqueropanyo, O.-A.; Naksata, W.; Sooksamiti, P. Preparation of anion exchange resin loaded with ferric oxide for arsenic (V) removal from aqueous solution. *Int. J. Environ. Sci. Dev.* **2017**, *8*, 399–403, https://doi.org/10.18178/ijesd.2017.8.6.985.

23. Hami, H.K.; Abbas, R.F.; Waheb, A.A.; Abed, M.A.; Maryoosh, A.A. Isotherm and pH Effect Studies of Tetracycline Drug Removal from Aqueous Solution Using Cobalt Oxide Surface. *Nahrain J. Sci.* **2019**, *22*, 12–18, https://doi.org/10.22401/anjs.22.2.02.

24. Ngapa, Y.D.; Gago, J. Optimizing of Competitive Adsorption Methylene Blue and Methyl Orange using Natural Zeolite from Ende-Flores. *J. Kim. Pendidikan Kim.* **2021**, *6*, 39-48, https://doi.org/10.20961/jkpk.v6i1.46132.

25. Liaqat, S.; Ibrahim, T.H.; Khamis, M.I.; Nancarrow, P.; Abouleish, M.Y. Clay-Alginate Beads Loaded with Ionic Liquids: Potential Adsorbents for the Efficient Extraction of Oil from Produced Water. *Polymers* **2022**, *14*, 4440, https://doi.org/10.3390/polym14204440.

26. Saruchi; Verma, R.; Kumar, V.; Alothman, A.A. Comparison between removal of Ethidium bromide and eosin by synthesized manganese (II) doped zinc (II) sulphide nanoparticles: kinetic, isotherms and thermodynamic studies. *J. Environ. Health Sci. Eng.* **2020**, *18*, 1175-1187, https://doi.org/10.1007%2Fs40201-020-00536-2.

27. López, J.n.E.; Builes, S.; Heredia Salgado, M.A.; Tarelho, L.A.C.; Arroyave, C.; Aristizábal, A.; Chavez, E. Adsorption of cadmium using biochars produced from agro-residues. *J. Phys. Chem. C.* **2020**, *124*, 14592–14602, https://doi.org/10.1021/acs.jpcc.0c02216.

28. Eduah, J.O.; Nartey, E.K.; Abekoe, M.K.; Henriksen, S.W.; Andersen, M.N. Mechanism of orthophosphate (PO_4-P) adsorption onto different biochars. *Environ. Technol. Innov.* **2020**, *17*, 100572, https://doi.org/10.1016/j.eti.2019.100572.

29. Zeng, Z.-w.; Tian, S.-r.; Liu, Y.-g.; Tan, X.-f.; Zeng, G.-m.; Jiang, L.-h.; Yin, Z.-h.; Liu, N.; Liu, S.-b.; Li, J. Comparative study of rice husk biochars for aqueous antibiotics removal. *J. Chem. Technol. Biotechnol.* **2018**, *93*, 1075-1084, https://doi.org/10.1002/jctb.5464.

30. Haque, A.N.A.; Uddin, M.K.; Sulaiman, M.F.; Amin, A.M.; Hossain, M.; Solaiman, Z.M.; Aziz, A.A.; Mosharrof, M. Combined Use of Biochar with [15]Nitrogen Labelled Urea Increases Rice Yield, N Use Efficiency and Fertilizer N Recovery under Water-Saving Irrigation. *Sustainability* **2022**, *14*, 7622, https://doi.org/10.3390/su14137622.

31. Joseph, C.G.; Anisuzzaman, S.M.; Sariah, A.; Musta, B.; Quek, K.S.; Wong, X.L. Adsorption Performance and Evaluation of Activated Carbon from Coconut Shell for the Removal of Chlorinated Phenols in Aqueous Medium. *Mater. Sci.* **2017**, *23*, 389-397, https://doi.org/10.5755/j01.ms.23.4.16221.

32. Bello, O.S.; Adelaide, O.M.; Hammed, M.A.; Popoola, O.A.M. Kinetic and equilibrium studies of methylene blue removal from aqueous solution by adsorption on treated sawdust. *Maced. J. Chem. Chem. Eng.* **2010**, *29*, 77-85, https://doi.org/10.20450/mjcce.2010.181.

33. Abdel-Galil, E.A.; Rizk, H.; El-kenany, W.M. Low cost natural adsorbent for removal of Pb(II) ions from waste solutions. *Arab J. Nucl. Sci. Appl.* **2018**, *51*, 19–30, https://doi.org/10.21608/ajnsa.2018.2340.1026.

34. Lasia, I.K. Carbon-Oxalate (C-Ox) Practicum Waste as an Adsorbent Material Candidate in the Chemistry Laboratory. *Molekul* **2022**, *17*, 421–427, https://doi.org/10.20884/1.jm.2022.17.3.6463.

35. Hussain, Z.; Sultan, N.; Ali, M.; Naz, M.Y.; AbdEl-Salam, N.M.; Ibrahim, K.A. Thermochemical Conversion of Waste Glass and Mollusk Shells into an Absorbent Material for Separation of Direct Blue 15 Azo Dye from Industrial Wastewater. *ACS Omega* **2020**, *5*, 18114-18122, https://doi.org/10.1021/acsomega.0c01680.

36. Nalwa, K.; Thakur, A.; Sharma, N. Synthesis of ZnO nanoparticles and its application in adsorption. *Adv. Mater. Proc.* **2021**, *2*, 697–703, https://doi.org/10.5185/amp/2017/696.

37. Yurmazova, T.; Shakhova, N.; Tuan, H.T. Adsorption of inorganic ions from aqueous solutions using mineral sorbent-Tripoli. *MATEC Web Conf.* **2016**, *85*, 01017, https://doi.org/10.1051/matecconf/20168501017.

38. Abdeen, Z.; Mohammad, S.G. Study of the Adsorption Efficiency of an Eco-Friendly Carbohydrate Polymer for Contaminated Aqueous Solution by Organophosphorus Pesticide. *Open J. Org. Polym. Mater.* **2014**, *4*, https://doi.org/10.4236/ojopm.2014.41004.

39. Yan, W.; Hoekman, S.K.; Broch, A.; Coronella, C.J. Effect of hydrothermal carbonization reaction parameters on the properties of hydrochar and pellets. *Environ. Prog. Sustain. Energy* **2014**, *33*, 676–680, https://doi.org/10.1002/ep.11974.

40. Rahman, M.L.; Fui, C.J.; Ting, T.X.; Sarjadi, M.S.; Arshad, S.E.; Musta, B. Polymer Ligands Derived from Jute Fiber for Heavy Metal Removal from Electroplating Wastewater. *Polymers* **2020**, *12*, 2521, https://doi.org/10.3390/polym12112521.

41. Pang, X.; Yang, C.; Ren, S. Adsorption Capacity of Expansion Graphite for Xylenol Orange. *J. Mater. Sci. Chem. Eng.* **2013**, *1*, 1–5, https://doi.org/10.4236/msce.2013.11001.

42. Shirmardi, M.; Mesdaghinia, A.; Mahvi, A.H.; Nasseri, S.; Nabizadeh, R. Kinetics and Equilibrium Studies on Adsorption of Acid Red 18 (Azo-Dye) Using Multiwall Carbon Nanotubes (MWCNTs) from Aqueous Solution. *J. Chem.* **2012**, *9*, 2371–2383, https://doi.org/10.1155/2012/541909.

43. Yusuff, S.M.; Khim, O.K.; Yunus, W.M.Z.W.; Fitrianto, A.; Ahmad, M.B.; Ibrahim, N.A.; Osman, M.J.; Chuang, T.C. Adsorption kinetics and isotherm of methylene blue by thermally treated alum-based water treatment plant sludge. *Int. J. Adv. Appl. Sci.* **2017**, *4*, 89–93, https://doi.org/10.21833/ijaas.2017.012.018.

44. Geng, D.G. Removal of Nitrophenol from Water by Dodecyl Sulfate Modified Layered Double Hydroxides. *Asian J. Chem.* **2014**, *26*, https://doi.org/10.14233/ajchem.2014.15439.

45. Baltakys, K.; Zadaviciute, S.; Eisinas, A. Adsorption kinetic parameters of Fe3+ and Ni2+ ions by gyrolite. *Mater. Sci-Medzg* **2015**, *21*, 117–122, https://doi.org/10.5755/j01.ms.21.1.5735.

46. Fernandes, J.D.; Chaves, L.H.G.; Dantas, E.R.B.; Tito, G.A.; Guerra, H.O.C. PHOSPHORUS AVAILABILITY IN SOIL INCUBATED WITH BIOCHAR: ADSORPTION STUDY. *Rev. Caatinga* **2022**, *35*, 206–215, https://doi.org/10.1590/1983-21252022v35n121rc.

47. Thinakaran, E.; Brema, J.; Arumairaj, P.D. Feasibility of spent macroalgae biochar for removal of Acid Red 88 (AR) dye from its aqueous solution. *Global Nest J.* **2022**, *24*, 392–400, https://doi.org/10.30955/gnj.004322.

48. Zhu, Y.; Liang, H.; Yu, R.; Hu, G.; Chen, F. Removal of Aquatic Cadmium Ions Using Thiourea Modified Poplar Biochar. *Water* **2020**, *12*, 1117, https://doi.org/10.3390/W12041117.